COBEM 2023 27TH INTERNATIONAL CONGRESS OF MECHANICAL ENGENEERING

ABCM Brazilian Society of Mechanical Sciences and Engineering
27th ABCM International Congress of Mechanical Engineering
December 04-08, 2023, Florianópolis-SC, Brazil

COB-2023-0189
OPTIMIZING ISOGRID STRUCTURES FOR MULTIPLE PERFORMANCE CRITERIA: AN EXPERIMENTAL STUDY

Adrien Noel
Département des Sciences et Technologies, Haute École Condorcet, Belgium
noel.adrien@hotmail.com

Rafael Augusto Gomes
d2022103026@unifei.edu.br
Guilherme Ferreira Gomes
Mechanical Engineering Institute, Universidade Federal de Itajubá (UNIFEI), Itajubá, Brazil
guilhermefergom@unifei.edu.br

Abstract. *The use of lattice structures has increased in several sectors due to the potential for mass reduction without significant rigidity loss. Originally designed for the aerospace sector, Isogrid structures have proven effective in significantly reducing mass without compromising rigidity. With the advancement of additive manufacturing technology, this contributed to the development of these complex structures, facilitating their applications in other sectors, such as the development of human prostheses. Since then, the subject has gained more visibility in the literature. The current paper aims to investigate and evaluate the behavior of the Isogrid tubular structure performance in the compression test, comparing the efficiency of the Isogrid tube multi-objective optimization considering six objectives to the non-optimized Isogrid structure. These samples were fabricated using a 3D printer utilizing two different materials: PLA and carbon filament. Six samples of each model were produced, evenly divided between PLA and carbon filament compositions. The compression tests were conducted using a universal testing machine, allowing for the evaluation of force versus displacement, energy absorption (EA) versus displacement, specific energy absorption (SEA), and the primary crushing force. The test results facilitated a comparison of the efficiency between the optimized and non-optimized structures manufactured with different materials. Although the optimized structure was slightly heavier with less than a 20% difference, it withstood over 100% more force compared to the non-optimized structure.*

Keywords: *Isogrid; Tubular Structure, Additive manufacturing, Optimization*

1. INTRODUCTION

Isogrid structures were initially developed for the aerospace industry, effectively reducing weight while maintaining structural rigidity. The emergence of additive manufacturing technology has played a significant role in advancing these intricate structures, enabling their application in various fields, including the development of prosthetic limbs. As a result, the subject has garnered increased attention in academic literature (Francisco *et al.*, 2021).

A majority of the studies focus on the fabrication process and manufacturing of Isogrid structures, with an emphasis on experimental testing. Forcellese *et al.* (2020) utilized 3D printing to create lattice panels made of carbon fiber-reinforced polyamide. The researchers investigated the impact of geometric parameters on compressive strength and buckling performance. Similarly, Li *et al.* (2019) employed additive techniques to construct a hierarchical Isogrid tube and assess its resistance to buckling and plastic deformation. Ciccarelli *et al.* (2021) also utilized 3D printing to manufacture six Isogrid panels, varying rib width and rib thickness, to examine the influence of geometric parameters on compressive loads. The authors concluded that increasing rib width enhances strength.

Li & Fan (2018) fabricated Isogrid stiffened cylinders using carbon fiber to investigate failure modes. Their findings indicated that skin thickness, cell dimension, rib height, rib thickness, and end strengthening scheme collectively determine the failure pattern. Similarly, Bellini *et al.* (2021) produced an Isogrid stiffened cylinder with identical geometry and compared it to another made of titanium alloy. The authors determined that the composite material exhibited equivalent stiffness and strength while being lighter.

Other researchers have proposed numerical analyses of Isogrid structures using the finite element method (FEM). Liang *et al.* (2020) put forth a numerical model for thin-walled Isogrid-stiffened cylinders, examining their structural buckling behavior under imperfections and employing reduced-order modeling. The researchers concluded that their proposed method yielded favorable results. In a study by Junqueira *et al.* (2019), the performance of Isogrid structures under compression and torsion loads was investigated using both numerical and experimental approaches. The authors demonstrated that their proposed model outperformed conventional prosthetic tubes.

While the aforementioned studies have made valuable contributions to understanding the fabrication process and the influence of design variables on Isogrid structures, none of them have focused on optimization. Only a limited number of studies have explored this aspect in the existing literature. This article addresses the evaluation of optimized tubular Isogrid structures.

In this experimental study, we aim to optimize Isogrid structures considering multiple performance criteria. Lattice structures have gained popularity in various sectors due to their potential for reducing mass without compromising rigidity. Initially developed for the aeronautical industry, Isogrid structures have found applications in diverse fields, including the development of human prostheses, thanks to advancements in additive manufacturing technology. As the subject gains increasing visibility in the literature, our research focuses on investigating and evaluating the performance of Isogrid tubular structures under compression testing. Specifically, we compare the efficiency of multi-objective optimization for Isogrid tube structures to non-optimized counterparts. The samples used in our study have identical parameters of diameter and height, and we analyze their efficiency based on weight. Our findings reveal that the optimized structures, with an average weight of 25 grams, outperformed the non-optimized structures, which weighed an average of 21 grams. The samples were manufactured using a 3D printer with PLA and carbon filament materials, and comprehensive testing was conducted using a universal testing machine. The results provide valuable insights into the force-displacement relationship, energy absorption, specific energy absorption, and main crushing force of the optimized and non-optimized structures.

2. THEORETICAL BACKGROUND

2.1 Isogrid Structures

Isogrid structures represent a class of lightweight, high-strength structural configurations that have garnered significant attention in various engineering applications. These structures are characterized by a regular lattice framework consisting of interconnected ribs or trusses, forming a continuous network. The Isogrid design offers remarkable advantages, primarily in terms of mass reduction while maintaining structural rigidity, making it an attractive choice for industries where weight optimization is crucial.

Advancements in additive manufacturing technologies, such as 3D printing, have significantly contributed to the development and widespread utilization of Isogrid structures. The additive manufacturing process allows for the fabrication of complex geometries with high precision, making it feasible to produce intricate lattice structures that were once challenging to manufacture using traditional methods. This technological progress has expanded the applications of Isogrid structures beyond the aeronautical industry, finding use in areas such as automotive, aerospace, civil engineering, and even biomedical fields, including the development of prosthetic devices.

The structural performance of Isogrid structures is influenced by various design parameters, including the size, shape, and orientation of the lattice cells, as well as the thickness and material properties of the connecting ribs. Research efforts have been dedicated to understanding the mechanical behavior and optimizing the performance of Isogrid structures. Studies have focused on investigating factors such as load-bearing capacity, stiffness, buckling behavior, energy absorption, and failure modes.

Isogrid structures can be just the rigid ribs or can be the rigid ribs cover with a coating, the first model is used in this paper and is called open. The second is called close. Eight variables can be used to describe the structure, they are: angle between helical ribs (φ), width of circular (δ_c) and helical (δ_h) ribs, thickness (h), length (L), diameter (D), distance of circular (α_c) and helical (α_h) sleepers from the structure axis. The first three are the main ones in the design of the Isogrid tube and that is why they are the decision variables in this study. They are represented in Figure 1.

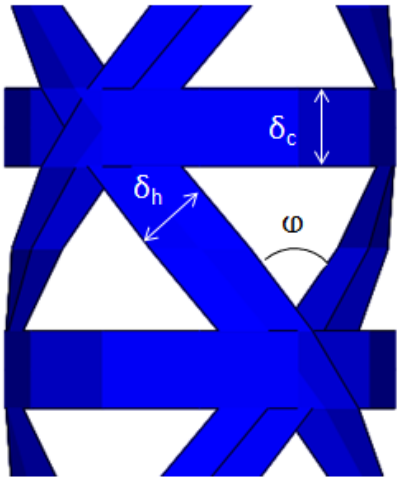

Figure 1. Geometric parameters of the Isogrid tube (adapted from Pereira *et al.*, 2022).

2.2 Multi-Objective Lichtenberg Optimization Algorithm

Meta-heuristics are algorithms capable of assimilating decision variables and utilizing the acquired knowledge to navigate towards optimal regions. These algorithms do not necessarily rely on a predefined function and can evaluate output responses through specialized software, such as Finite Element Method (FEM). The ability of meta-heuristics to learn from decision variables and escape non-optimal regions and local minima categorizes them as Artificial Intelligence algorithms. While conventional optimization methods may struggle with multimodal, non-convex problems with numerous decision variables, meta-heuristics provide effective solutions. Inspired by natural phenomena, each meta-heuristic algorithm incorporates parameters that control its exploration and exploitation capabilities based on its source of inspiration (Mirjalili, 2016; Pereira, *et al.* 2022).

Due to the No-free-lunch (NFL) theorem, there is no single algorithm that excels in all applications. As a result, the pursuit of novel and powerful algorithms remains constant. Modern problem operators seek to generate as many solutions as possible before deciding which ones to adopt. The Lichtenberg Algorithm, inspired by lightning propagation in resistant media, introduced a novel approach by considering trajectory and population simultaneously. The algorithm generates fractal-like patterns called Lichtenberg Figures, which have found successful applications in crack identification, damage assessment in composites, and the optimization of Isogrid tube designs using metamodels. Building upon the single-objective version, the recently published Multi-objective Lichtenberg Algorithm (MOLA) will be utilized in this study.

In the MOLA, a Lichtenberg figure is introduced into the search space with varying rotations and sizes across Niter iterations. The creation of the Lichtenberg figure involves three key parameters: the creation radius (*Rc*), the number of particles (*Np*), and the stickiness coefficient (*S*). The stickiness coefficient influences the density of the generated Lichtenberg figure, while the first two parameters relate to its size. Within the figure, a set number of points are randomly selected and evaluated using objective functions, yielding solutions in the search space. These solutions are compared using the Pareto dominance relationship, allowing for the formation and updating of a partial Pareto front at each iteration. The Lichtenberg figure launched in each iteration is centered on a randomly selected point from the current Pareto front. The *ref* parameter, if nonzero, generates a smaller Lichtenberg figure at a rate specified by *ref*. Half of the Pop points are required to reside within this smaller figure, potentially enhancing the accuracy and convergence of the algorithm. Figure 2 illustrates the behavior of the Lichtenberg Algorithm in the search space across iterations, along with its corresponding convergence in the objective space. Figure 3 provides a concise summary of the algorithm's operation.

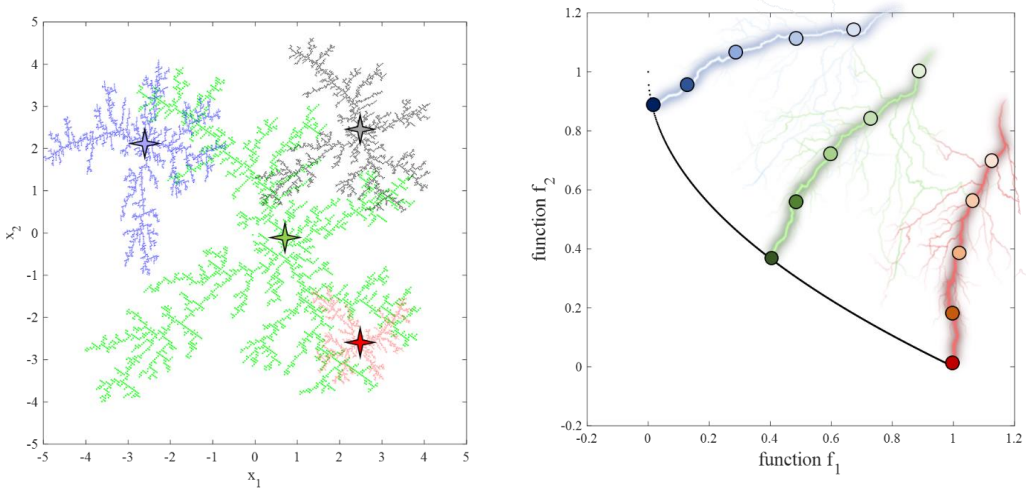

(a) (b)

Figure 2. Basic search strategy of MOLA in the design and objective space (adapted from Pereira *et al.*, 2022).

3. METHODOLOGY

3.1 Numerical Model

Francisco *et al.* (2020) studied an Isogrid numerical model and made comparisons with experimental tests to find the best fits. The results found by the authors showed that the numerical approach is in accordance with the experiments. Therefore, in this paper will be used the same shell element with 8 nodes and six degrees of freedom.

The Isogrid model proposed is made with CFRP T300/epoxy. This material was analyzed by Madhavi (2009). The author carried out experimental tests for its characterization and the parameters is shown in Tab 1. This data was used by Francisco *et al.* (2020 & 2021) for a prosthetic tube numerical analysis.

Table 1. Experimental Properties of T300 Carbon Fiber/Epoxy Resin (adapted from Madhavi, 2009).

Propriety	Unit	Value	Standard
E_1	GPa	144	ASTM D3039
E_2	GPa	6.5	ASTM D3039
G_{12}	GPa	5.6	ASTM D3518
S_{12}	MPa	40	ASTM D3518
σ_1^T	MPa	1200	ASTM D3039
σ_2^T	MPa	17	ASTM D3039
σ_1^C	MPa	600	ASTM D3410
σ_2^C	MPa	80	ASTM D3410
ILSS	MPa	42	ASTM D2344
ρ	kg/m³	1350	ASTM D3039
υ_{12}	-	0.21	ASTM D3039

The Isogrid tube is formed by 7 sheets of 0.2mm each, i.e., the total thickness of the model is equal to 1.4mm. This value was adopted by Junqueira *et al.* (2019) and shows excellent results in experimental tests. In addition, it is important to highlight that the carbon fibers orientation is shown in Fig. 3(b). For the numerical analysis, the force and the moment were applied at the end of the structure while the other side is clamped as shown in Fig. 3(a). The loads used in this numerical model are according to the standard that have norms to lower limbs prosthesis structural testing (NBR ISO 10328: 2002). The adopted loads are 4480 N for compression.

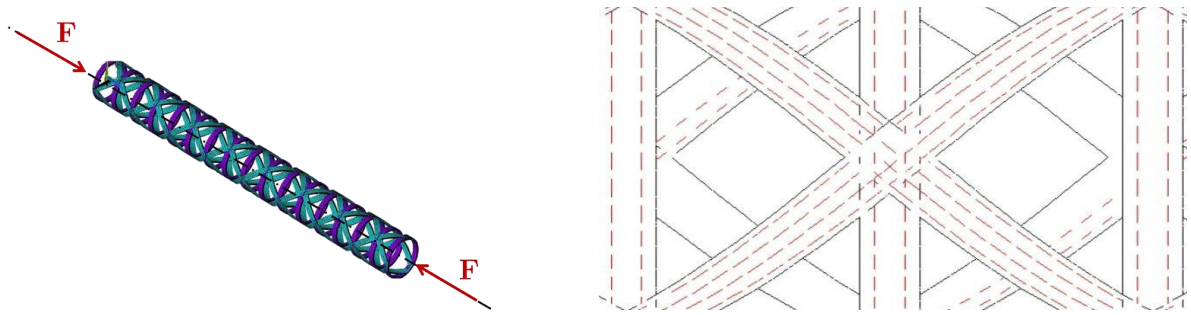

(a) (b)

Figure 3. Boundary conditions applied to the model for (a) compression test and (b) torsion cases.

3.2 Multi-objective Optimization of Isogrid Tubes

The optimization problem modeling is similar to the previous one and is expressed in Equation 1.

$$\begin{aligned} &\textit{Find } \boldsymbol{X} = \{\boldsymbol{\varphi}, \boldsymbol{\delta_h}, \boldsymbol{\delta_c}\} \textit{ that} \\ &\textit{minimizes } F(\boldsymbol{X})=\{\boldsymbol{M(X)}, -\boldsymbol{\lambda_C(X)}, \boldsymbol{TW_C(X)}\} \\ &\textit{subject to:} \\ &\quad 20 \leq \boldsymbol{\varphi} \leq 50\ [°] \\ &\quad 2 \leq \boldsymbol{\delta_h} \leq 6\ [mm] \\ &\quad 2 \leq \boldsymbol{\delta_c} \leq 6 [mm] \end{aligned} \tag{1}$$

3.3 Experimental Testing

In this experimental study, the specimens were manufactured using additive manufacturing techniques 3D printing through the FDM process. The original numerical study (Francisco *et al.*, 2021; Pereira *et al.*, 2022) has the Isogrid structure of composite material. Here, the structure is achieved by means of PLA and PLA with Carbon filament materials. Although the material is not the same as in the numerical study, the proposed methodology will be useful to compare the initial structural (non-optimized) with that obtained through the multi-objective optimization.

Figure 4 shows the manufacturing process for Isogrid tubes. As parameters of the construction process, diameter of 1.75mm, Infill speed = 30 mm/s, printing temperature = 200°C, build plate temperature = 60°C, layer height = 0.2mm were used. Where the material properties such as the Young modulus and Poisson's ratio obtained by the experimental test from the ASTM D695 were respectively 1,408E+9 and 0,33 from PLA, as well as 1,213E+9 and 0,31 from PLA+Carbon.

Finally, Figure 5 shows the already manufactured Isogrid structures. As a sampling, 3 structures were obtained for each configuration and for each material, that is, 12 Isogrid tubes in total.

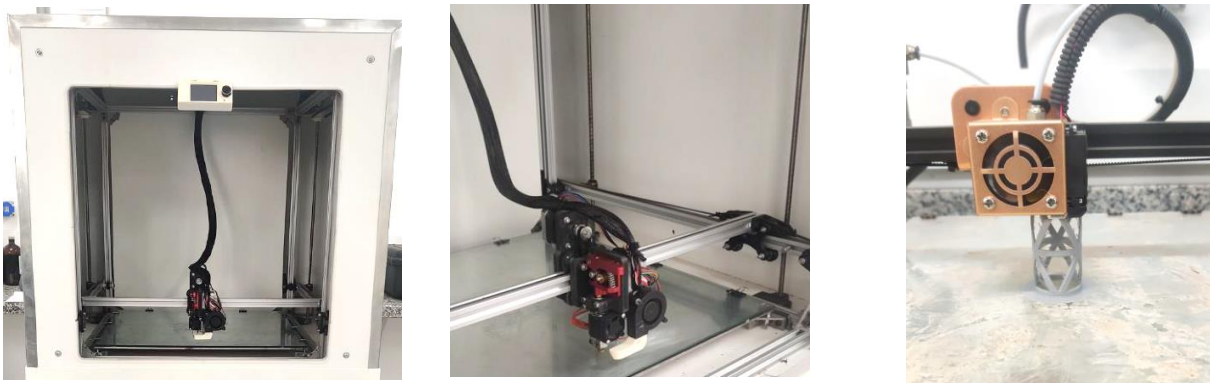

(a) (b)

Figure 4. (a) Manufacturing using FDM process and (b) printing detail of an Isogrid tube.

(a) PLA (b) PLA optimized (c) PLA-Carbon (d) PLA-Carbon optimized

Figure 4. Isogrid tubular structures (normal and optimized) obtained through FDM process.

4. RESULTS AND DISCUSSION

4.1 Numerical Results

The Pareto front generated for the optimization problems in Eq.1 is shown in Fig. 5. It is possible to see the non-dominated solutions and the best solution found using the Technique for Order of Preference by Similarity to ideal Solution (TOPSIS) for the MOLA-FEM and MOLA-RSM methodologies.

TOPSIS was the decision-making technique. The method uses the utopia point as positive ideal solution (A+) and the nadir point as negative ideal solution (A-) to calculate a score for each solution in Pareto front. The utopia point is an imaginary point composed of the imaginary minima of each objective, while the Nadir point is exactly the opposite. Using Euclidian distance, it determines which solution is the closest to (A+) and the furthest from (A-). Still, the method can be accompanied by tools for normalization of the search space, so that objectives that have larger ranges are not favored. Also, weights can be used to increase the importance of some objectives.

The main motivation for using the two methodologies is to compare the accuracy of the results. In terms of computational cost, each simulation using FEM takes about 40s. In the LA-RSM methodology, there are 20 experiments, which generates a 13 minutes simulation time. In the LA-FEM, there are 40 × Pop × Niter experiments, which results in approximately 55h.

For the LA-RSM in all cases, the Pareto fronts have more consistency and continuity, given the optimization generated by second-order polynomial equations. However, it is possible to observe that the Isogrid structure optimization true nature have discontinuous Pareto fronts.

Table 3 displays the final result of the multi-objective optimization in contrast to the baseline (or normal) model. The solution determined by the TOPSIS algorithm was taken as the optimal point of the Pareto front.

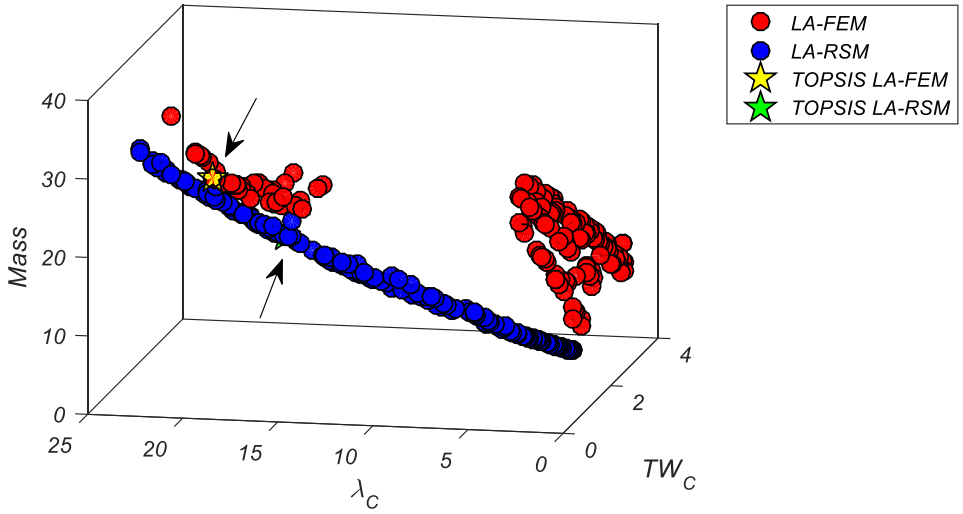

Figure 5. Multi-objective optimization results and Pareto surface for the Isogrid tube.

Table 2. Baseline (normal) and optimized Isogrid parameters.

	φ (°)	*δh (mm)*	*δc (mm)*
Normal	40.00	4.00	4.00
Optimized	25.07	6.00	4.13

4.2 Experimental Results

After the execution of the experimental compression tests, the results of force-displacement were obtained directly and properties of absorbed energy (EA), specific absorbed energy (SEA) and main crushing force (MSF). For measuring the energy absorption (*EA*), some authors have proposed to characterize the energy absorption capabilities of the inner tube during the axial crushing test, which can be mathematically calculated by the Eq. 2.

$$EA = \int_0^{\delta} F(s)ds \quad [J] \tag{2}$$

where *F(s)* is the instantaneous crushing force in the impact direction, and is the stroke distance. To calculate the Specific Energy Absorption (*SEA*), it is proposed to represent the energy absorption (*EA*) per mass (*M*) (Eq. 3).

$$SEA = \frac{EA}{M} \quad [J/g] \tag{3}$$

In addition, the energy absorption per loading displacement (*d*) is defined in order to calculate the main crushing force (*MCF*) of the Isogrid structure (Eq. 4).

$$MCF = \frac{EA}{d} \quad [kN] \tag{4}$$

Figures 6 and 7 show the force-displacement result of the compression test for PLA and PLA carbon tubes. First, the results exhibit substantial reproducibility, with a small standard deviation between replicates, which characterizes an adequate additive manufacturing process. This result was more prominent in the PLA specimens. For both materials, the superiority in terms of resistance of the optimized structures is clearly observed. Furthermore, this resistance gain resulted

in a slight loss of total displacement. Complementarily, Fig. 8 shows the failure mode of the structures after the compression test.

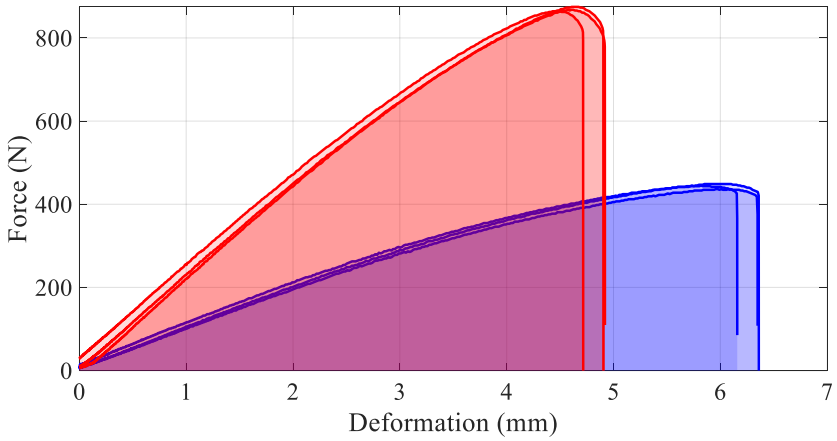

Figure 6. Compression results for the normal and optimized Isogrid tubes for all the three replicates for PLA material (legend: — normal and — optimized).

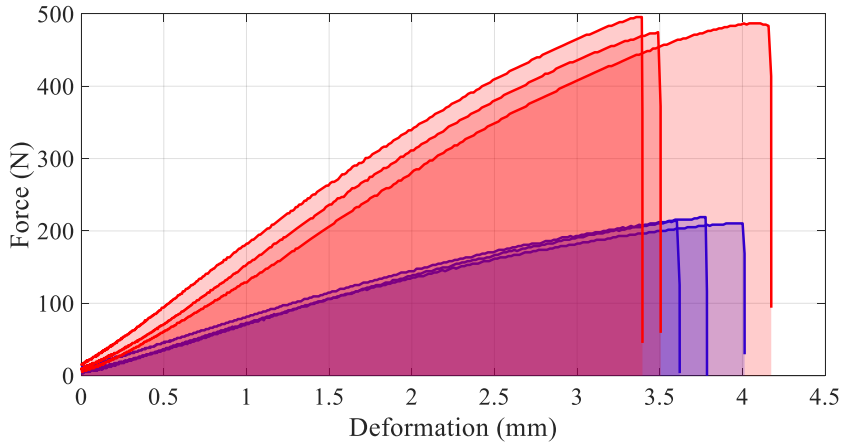

Figure 7. Compression results for the normal and optimized Isogrid tubes for all the three replicates for PLA+Carbon material (legend: — normal and — optimized).

(a) PLA (b) PLA + Carbon

Figure 8. Failure mode of Isogrid tubes after compression test.

Figure 10, in turn, compares the non-optimized and optimized structures grouped for different materials. At this point, it is clear that the PLA filament has a huge structural advantage over the PLA material with the carbon insert. The advantage is in both force and displacement properties, as shown in the Force-displacement diagram.

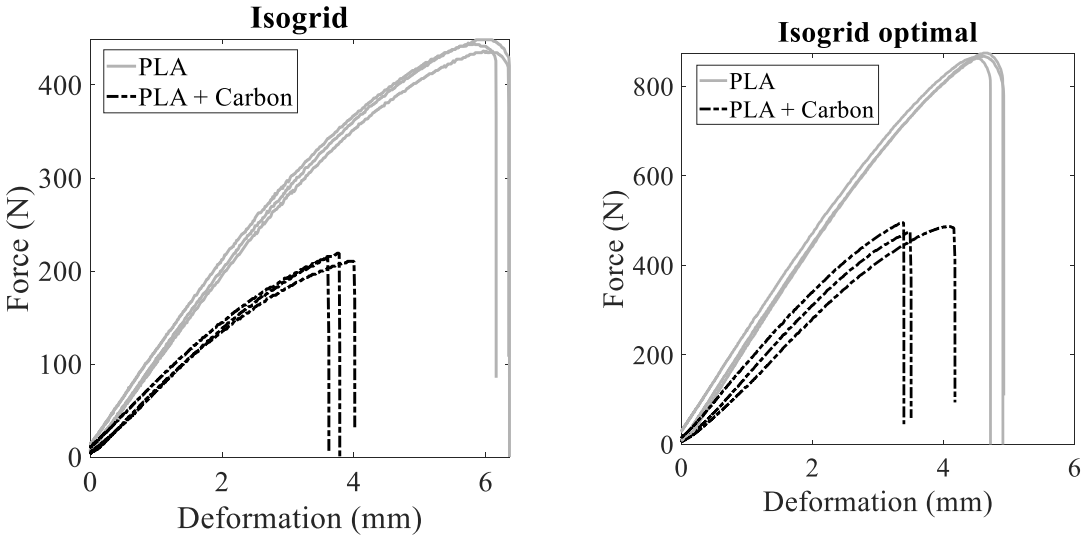

(a) (b)

Figure 9. Compression results for the normal and optimized Isogrid tubes for all the three replicates for different materials (PLA and PLA+Carbon).

Equally important, Fig. 11 shows the result obtained through Eq. (2) for the energy absorbed by structures. Once again, the optimized structures, despite having less total displacement, are capable of absorbing more energy. This result was more evident for structures manufactured from PLA with carbon.

Figure 12 groups the same result in comparison of different materials. As discussed in the previous paragraph, the PLA filament also has an advantage over the PLA filament with carbon.

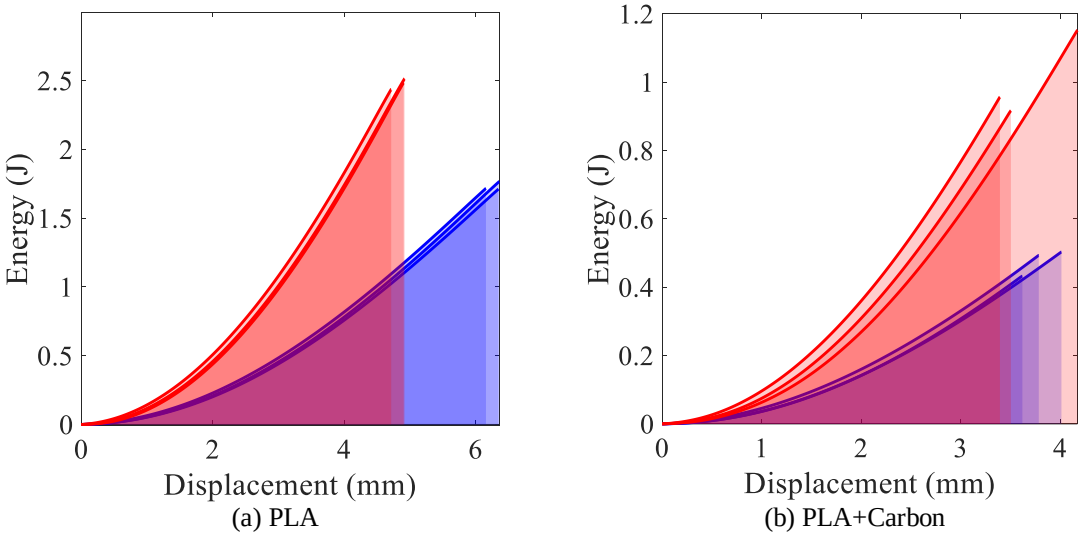

(a) PLA (b) PLA+Carbon

Figure 10. Energy absorbed (EA) results for the normal and optimized Isogrid tubes for all the three replicates for different materials (legend: — normal and — optimized).

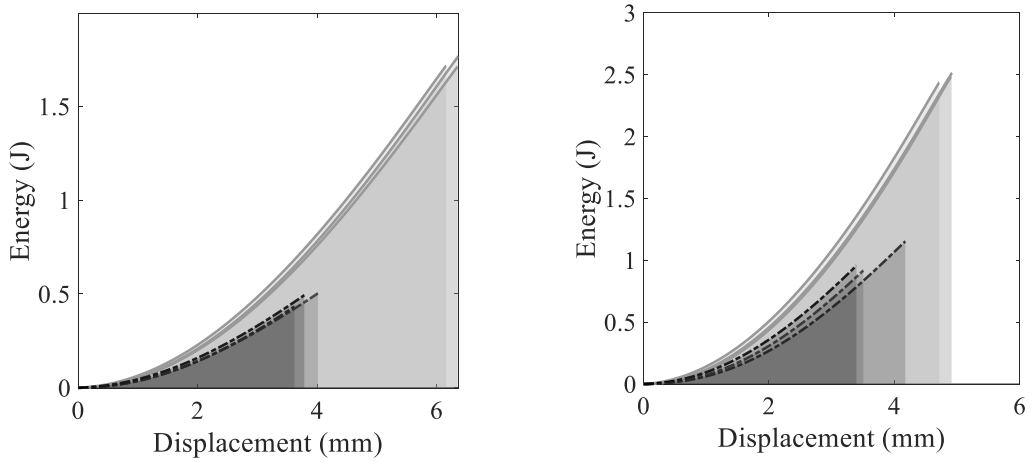

(a) normal (b) optimized

Figure 11. Energy absorbed (EA) results for the normal and optimized Isogrid tubes for all the three replicates for different materials (legend: ▬ PLA and ▪▪▪ PLA+Carbon).

Finally, Tables 4 and 5 group the results extracted from the Force-displacement signal for the structures tested in triplicate. Briefly, Tab. 6 displays the result of the average of the three tested structures. From the extracted data, it can be said that in general the optimized model (numerically) was confirmed by means of the experimental tests. In general, the optimized models showed a mass increase of less than 20% compared to the non-optimal one, however, this mass increase led to a 126% increase in the failure force (for the PLA material with carbon).

It can also be said from the data obtained that the optimized model lost total displacement capacity (which was already expected), but gained several other advantages in its structural properties.

Table 3. Experimental results considering PLA Isogrid structure.

	Normal			Optimized		
Replicate	1	2	3	1	2	3
Mass (g)	20.75	20.76	20.74	24.67	24.87	24.89
Max. displacement (mm)	6.3602	6.3489	6.1584	4.7165	4.9058	4.9198
Max force (N)	448.64	436.47	445.17	864.25	874.68	867.73
Specific force (N/g)	21.6212	21.0246	21.4643	35.0324	35.1701	34.8626
EA (J)	1.7661	1.7113	1.7166	2.4363	2.4858	2.5142
SEA (J/kg)	85.1146	82.4348	82.7680	98.7568	99.9500	101.0131
MCF (N)	277.6844	269.5501	278.7427	516.5547	2.4858	2.5142

Table 4. Experimental results considering PLA w/ Carbon Isogrid structure.

	Normal			Optimized		
Replicate	1	2	3	1	2	3
Mass (g)	21.7580	21.7120	21.6740	25.9710	25.9800	25.0500
Max. displacement (mm)	4.0132	3.6206	3.7857	3.5055	4.1744	3.3953
Max force (N)	210.41	213.89	219.11	474.73	486.90	495.60
Specific force (N/g)	9.6705	9.8512	10.1093	18.2792	18.7413	19.7844
EA (J)	0.5030	0.4324	0.4930	0.9168	1.1522	0.9566
SEA (J/kg)	23.1199	19.9166	22.7483	35.3018	44.3506	38.1871
MCF (N)	125.3468	119.4358	130.2393	261.5387	275.0226	281.7488

Table 5. Experimental average results for PLA and PLA+Carbon Isogrid Tubes.

	PLA			PLA + carbon		
Replicate	Normal	Optimized	Diff. (%)	Normal	Optimized	Diff. (%)
Mass (g)	20.7500	24.8100	+19.5663	21.7147	25.6670	+18.2012
Max. displacement (mm)	6.2892	4.8474	-22.9251	3.8065	3.6917	-3.0150
Max force (N)	443.4267	868.8867	+95.9482	214.47	485.7433	+126.4854
Specific force (N/g)	21.3700	35.0217	+63.8823	9.8770	18.9350	+91.7077
EA (J)	1.7313	2.4788	+43.1710	0.4761	1.0085	+111.8174
SEA (J/kg)	83.4391	99.9066	+19.7659	21.9283	39.2798	+79.1288
MCF (N)	275.3257	173.8516	-36.8560	125.0073	272.7700	+118.2033

5. CONCLUSIONS

In summary, this study investigated the performance of optimized Isogrid tubular structures compared to non-optimized ones through compression testing.

The results showed that the optimized structures exhibited greater strength and energy absorption capabilities while experiencing a slight decrease in total displacement. The addition of carbon filament did not significantly enhance the structural properties of the Isogrid structures compared to pure PLA filament.

Overall, the findings support the feasibility of multi-objective optimization for Isogrid structures, highlighting their potential for lightweight and robust applications in industries such as aerospace and prosthetics. Future research can further explore optimization techniques and materials to improve the efficiency of Isogrid structures.

6. ACKNOWLEDGEMENTS

The authors would like to acknowledge the financial support from the Brazilian agency CNPq (Conselho Nacional de Desenvolvimento Cientifico e Tecnológico - 431219/2018-4), CAPES (Coordenação de Aperfeiçoamento de Pessoal de Nível Superior) and FAPEMIG (Fundação de Amparo à Pesquisa do Estado de Minas Gerais - APQ-00385-18).

7. REFERENCES

Bellini, C., Di Cocco, V., Iacoviello, F., & Sorrentino, L. (2021). Performance index of Isogrid structures: robotic filament winding carbon fiber reinforced polymer vs. titanium alloy. Materials and Manufacturing Processes, 1–9.

Ciccarelli, D. Archimede Forcellese, Luciano Greco, Tommaso Mancia, Massimiliano Pieralisi, Michela Simoncini, Alessio Vita. Buckling behavior of 3D printed composite Isogrid structures. Procedia CIRP. Volume 99, 2021, Pages 375-380, ISSN 2212-8271.

Forcellese, Archimede *et al.* Manufacturing of Isogrid Composite Structures by 3D Printing. Procedia Manufacturing, v. 47, p. 1096-1100, 2020.

Francisco, M. F., Pereira, J. L. J., *et al.* Multiobjective design optimization of CFRP Isogrid tubes using sunflower optimization based on metamodel. Computers & Structures. Vol. 249. June 2021, 106508.

Junqueira, Diego Morais *et al.* Design optimization and development of tubular Isogrid composites tubes for lower limb prosthesis. Applied Composite Materials, v. 26, n. 1, p. 273-297, 2019.

Li, C. Lai, Q. Zheng, *et al.*, Design and mechanical properties of hierarchical Isogrid structures validated by 3D printing technique. Materials & Design, https://doi.org/10.1016/j.matdes.2019.107664

Li, Ming; Fan, Hualin (2018). Multi-failure analysis of composite Isogrid stiffened cylinders. Composites Part A: Applied Science and Manufacturing.

Liang, Ke; Yang, Chen; Sun, Qin (2020). A smeared stiffener based reduced-order modelling method for buckling analysis of Isogrid-stiffened cylinder. Applied Mathematical Modelling, 77(), 756–772.

Pereira, J. L. J., Francisco, M. B., Ribeiro, R. F., Cunha, S. S., & Gomes, G. F. (2022). Deep multiobjective design optimization of CFRP Isogrid tubes using lichtenberg algorithm. Soft Computing, 26(15), 7195-7209.

Mirjalili S, Saremi S, Mirjalili SM, Coelho LDS. Multi-objective grey wolf optimizer: A novel algorithm for multi-criterion optimization. Expert Syst Appl 2016;47:106–19.

8. RESPONSIBILITY NOTICE